Electronic Supplementary Material (ESI) for Dalton Transactions.


# Electronic Supplementary Information

## Controllable Syntheses and Magnetic Properties of Novel Homoleptic Triple-decker Lanthanide Complexes†

Feng Gao,*[a] Lei Wang,*[b] Guang-Zhou Zhu,[a] Yu-Han Liu,[a] Han Yang,[a] Xiang Li[a] and Ke Yang[a]

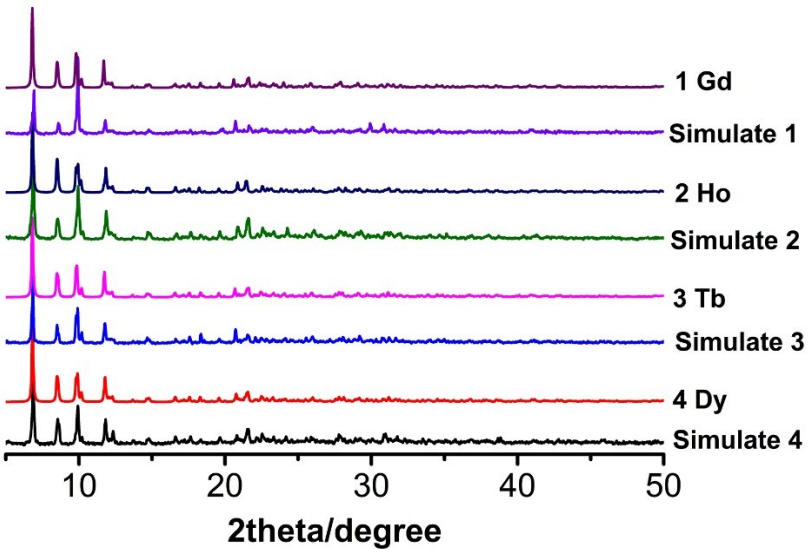


**Fig. S1** Experimental and simulated PXRD patterns of complexes **1**–**4**.

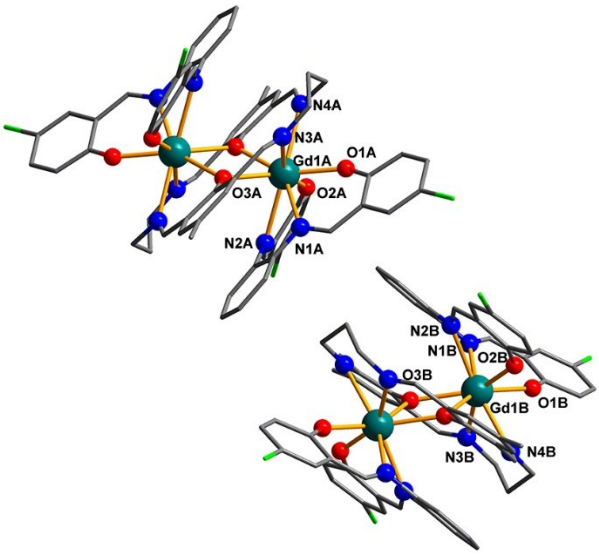


**Fig. S2** Molecular structure of Gd complex **1** with hydrogen atoms and solvent molecule omitted for clarity (Gd teal, N blue, Cl green, O red and C grey).

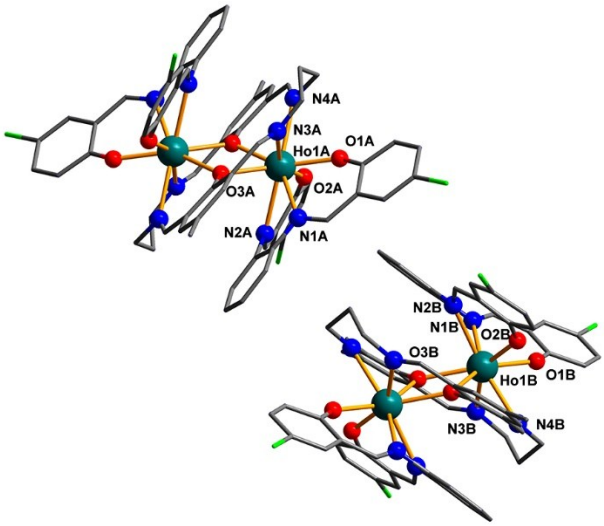


**Fig. S3** Molecular structure of Ho complex **2** with hydrogen atoms and solvent molecule omitted for clarity (Ho teal, N blue, Cl green, O red and C grey).

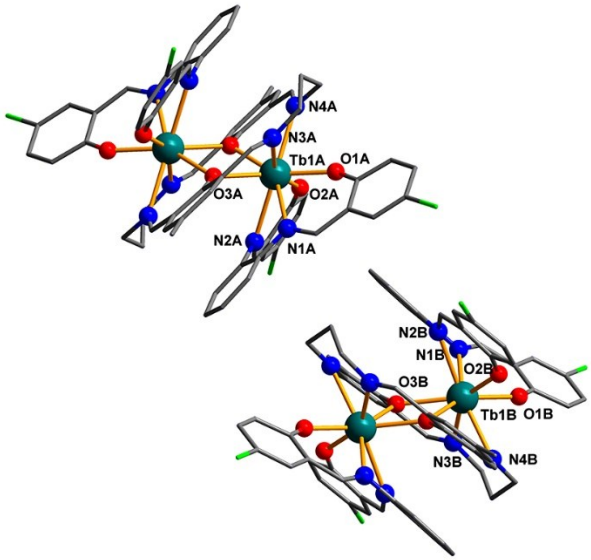


**Fig. S4** Molecular structure of Tb complex **3** with hydrogen atoms and solvent molecule omitted for clarity (Tb teal, N blue, Cl green, O red and C grey).

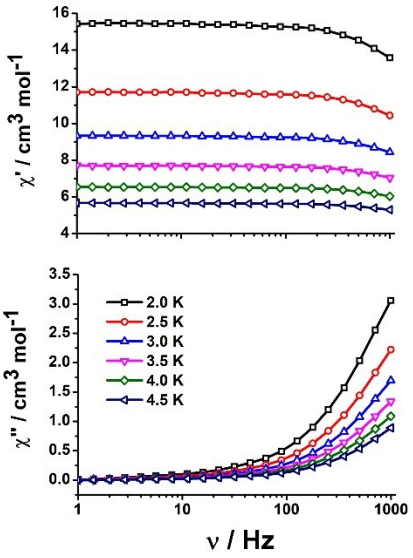


**Fig. S5** Frequency-dependent in-phase (χ') and out-of-phase (χ'') ac susceptibilities for Dy complex **4** from 2.0 to 4.5 K under $H_{dc}$ = 0 Oe.

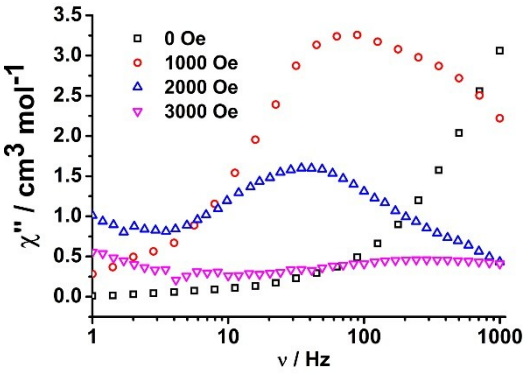


**Fig. S6** Frequency-dependence out-of-phase (χ'') ac susceptibilities for Dy complex **4** at 2.0 K under different external fields.

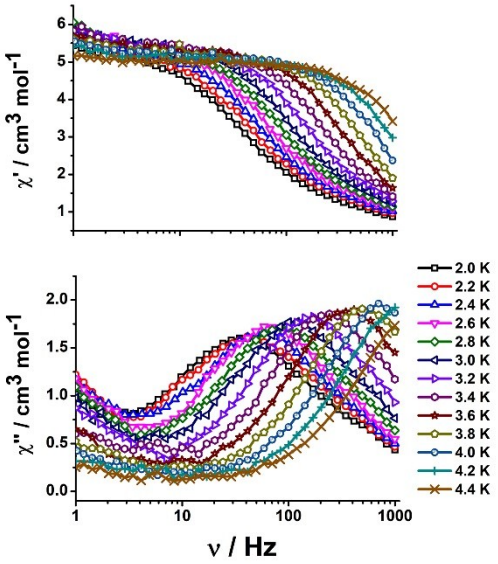


**Fig. S7** Frequency-dependent in-phase ($\chi'$) and out-of-phase ($\chi''$) ac susceptibilities of Dy complex **4** from 2.0 to 4.4 K under $H_{dc}$ = 2000 Oe.

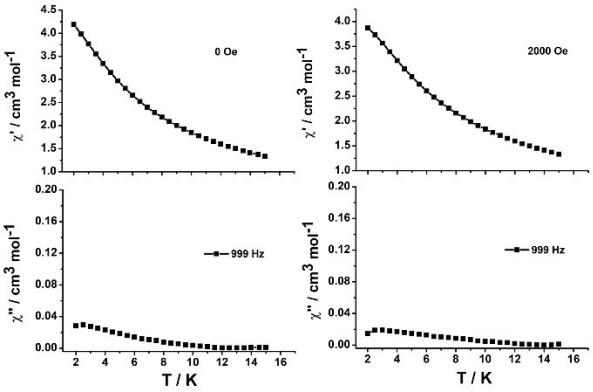


**Fig. S8** Temperature-dependent in-phase (χ′) and out-of-phase (χ′′) ac susceptibilities of Ho complex **2** at the frequency of 999 Hz under $H_{dc}$ = 0 Oe (left) and $H_{dc}$ = 2000 Oe (right).

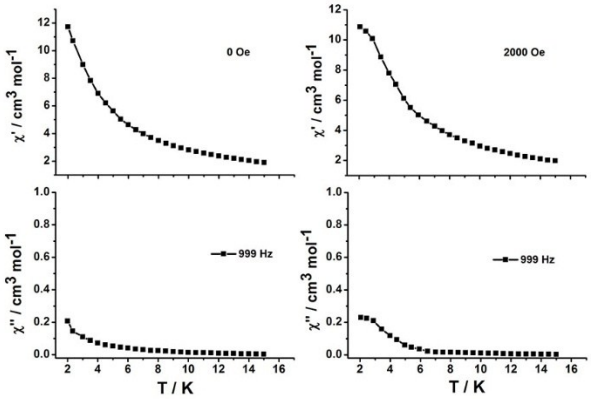


**Fig. S9** Temperature-dependent in-phase (χ′) and out-of-phase (χ′′) ac susceptibilities of Tb complex **3** at the frequency of 999 Hz under $H_{dc}$ = 0 Oe (left) and $H_{dc}$ = 2000 Oe (right).

**Table S1** Selected bond lengths (Å) and angles (°) for complexes **1**–**4**.

| | **1** | **2** | **3** | **4** |
|---|---|---|---|---|
| Ln(1A)-O(1A) | 2.256(3) | 2.218(3) | 2.233(4) | 2.227(3) |
| Ln(1A)-O(2A) | 2.253(4) | 2.220(3) | 2.239(5) | 2.224(4) |
| Ln(1A)-O(3A) | 2.358(3) | 2.331(3) | 2.344(4) | 2.334(3) |
| Ln(1A)-O(3A)#1[a] | 2.426(3) | 2.393(3) | 2.413(4) | 2.406(3) |
| Ln(1A)-N(1A) | 2.575(4) | 2.554(4) | 2.574(5) | 2.556(4) |
| Ln(1A)-N(2A) | 2.619(4) | 2.573(4) | 2.597(6) | 2.588(4) |
| Ln(1A)-N(3A) | 2.631(5) | 2.591(4) | 2.618(6) | 2.605(5) |
| Ln(1A)-N(4A) | 2.582(4) | 2.540(4) | 2.562(6) | 2.549(4) |
| Ln(1B)-O(1B) | 2.275(4) | 2.249(3) | 2.260(4) | 2.249(3) |
| Ln(1B)-O(2B) | 2.270(3) | 2.234(3) | 2.257(4) | 2.240(3) |
| Ln(1B)-O(3B) | 2.401(3) | 2.379(3) | 2.389(4) | 2.376(3) |
| Ln(1B)-O(3B)#2[a] | 2.425(3) | 2.406(3) | 2.410(4) | 2.405(3) |
| Ln(1B)-N(1B) | 2.537(4) | 2.521(4) | 2.530(5) | 2.518(4) |
| Ln(1B)-N(2B) | 2.568(4) | 2.523(4) | 2.548(5) | 2.535(4) |
| Ln(1B)-N(3B) | 2.605(4) | 2.560(4) | 2.577(5) | 2.574(4) |
| Ln(1B)-N(4B) | 2.548(4) | 2.508(4) | 2.532(5) | 2.514(4) |
| N(1A)-Ln(1A)-N(2A) | 61.61(14) | 62.15(12) | 61.93(17) | 61.88(13) |
| N(3A)-Ln(1A)-N(4A) | 75.27(15) | 75.72(13) | 75.70(19) | 75.59(15) |
| O(1A)-Ln(1A)-O(2A) | 85.03(14) | 82.78(13) | 84.17(17) | 83.32(14) |
| O(3A)-Ln(1A)-O(3A)#1[a] | 68.74(13) | 67.98(12) | 68.23(17) | 68.31(14) |
| Ln(1A)-O(3A)-Ln(1A)#1[a] | 111.26(13) | 112.03(12) | 111.77(17) | 111.69(14) |
| N(1B)-Ln(1B)-N(2B) | 62.88(14) | 63.22(12) | 62.35(17) | 62.96(14) |
| N(3B)-Ln(1B)-N(4B) | 76.20(14) | 76.50(13) | 76.11(17) | 76.27(14) |
| O(1B)-Ln(1B)-O(2B) | 81.84(13) | 80.69(11) | 81.26(16) | 81.16(13) |
| O(3B)-Ln(1B)-O(3B)#2[a] | 66.75(13) | 66.58(13) | 66.64(16) | 66.61(13) |
| Ln(1B)-O(3B)-Ln(1B)#2[a] | 113.25(13) | 113.42(13) | 113.36(16) | 113.39(13) |

[a] Symmetry transformations used to generate equivalent atoms: #1 -x+2,-y+1,-z+1 and #2 -x+1,-y+1,-z.

**Table S2** Summary of structural parameters for Dy complex **4**.

| | **4** |
|---|---|
| Average Dy-N bond length (Å) | 2.555 |
| Average Dy-O bond length (Å) | 2.307 |
| Dy(1A) to O(1A)-O(2A)-N(1A)-N(2A) plane center distance (Å) | 1.3583(3) |
| Dy(1A) to O(3A)-O(3A)#1-N(3A)-N(4A) plane center distance (Å) | 1.4044(3) |
| Dy(1B) to O(1B)-O(2B)-N(1B)-N(2B) plane center distance (Å) | 1.3473(3) |
| Dy(1B) to O(3B)-O(3B)#2-N(3B)-N(4B) plane center distance (Å) | 1.3897(3) |
| Dihedral angle between O(1A)-O(2A)-N(1A)-N(2A) and O(3A)-O(3A)#1-N(3A)-N(4A) planes (°) | 7.3075(9) |
| Dihedral angle between O(1B)-O(2B)-N(1B)-N(2B) and O(3B)-O(3B)#2-N(3B)-N(4B) planes (°) | 7.0883(8) |
| Shortest intermolecular $Dy^{3+}\cdots Dy^{3+}$ distance (Å) | 9.3684(6) |
| Intramolecular Dy(1A)-Dy(1A)#1 distance (Å) | 3.9231(5) |
| Intramolecular Dy(1B)-Dy(1B)#2 distance (Å) | 3.9963(5) |

**Table S3** Parameters obtained by continuous shape measurement (CShM) method for study of central Dy(III) coordination sphere of complex **4**. (The *S* values indicate the proximity to the selected ideal polyhedron, *S* = 0 corresponds to the non-distorted polyhedron).

| | $S_{Dy1A}$ | $S_{Dy1B}$ |
|---|---|---|
| Cube (CU, $O_h$) | 8.198 | 9.389 |
| Square antiprism (SAP, $D_{4d}$) | 1.385 | 0.994 |
| Triangular dodecahedron (TDD, $D_{2d}$) | 2.856 | 2.857 |

**Table S4** Relaxation fitting parameters of the Cole-Cole plots in high-frequency region based on the generalized Debye model[a] for Dy complex **4** under $H_{dc}$ = 2000 Oe in the temperature range of 2.0–4.4 K.

| T / K | $\chi_S$ / cm$^3$ mol$^{-1}$ | $\chi_T$ / cm$^3$ mol$^{-1}$ | ln($\tau$ / s) | α |
|---|---|---|---|---|
| 2.0 | 0.645 | 5.869 | -5.463 | 0.29 |
| 2.2 | 0.680 | 5.747 | -5.622 | 0.30 |
| 2.4 | 0.767 | 5.724 | -5.872 | 0.26 |
| 2.6 | 0.871 | 5.852 | -6.039 | 0.23 |
| 2.8 | 0.865 | 5.667 | -6.333 | 0.21 |
| 3.0 | 0.824 | 5.703 | -6.597 | 0.21 |
| 3.2 | 0.818 | 5.581 | -6.949 | 0.18 |
| 3.4 | 0.764 | 5.488 | -7.335 | 0.16 |
| 3.6 | 0.675 | 5.377 | -7.733 | 0.14 |
| 3.8 | 0.692 | 5.239 | -8.082 | 0.11 |
| 4.0 | 0.736 | 5.159 | -8.493 | 0.11 |
| 4.2 | 0.751 | 5.071 | -8.836 | 0.11 |
| 4.4 | 0.696 | 4.983 | -9.191 | 0.12 |

[a] $\chi_{total}(\omega) = \chi_S + \left[\frac{\chi_T - \chi_S}{1 + (i\omega\tau)^{1-\alpha}}\right]$

Where $\chi_S$ is the adiabatic susceptibility, $\chi_T$ is the isothermal susceptibility, ω (=2π$f$) is the angular frequency, $\tau$ represents the magnetization relaxation times.

**Computational details**

Complex **4** has two types of binuclear $Dy^{III}$ molecular structures indicated as **4_*a*** and **4_*b***. For each binuclear molecule, there is only one type of $Dy^{III}$ fragment due to its symmetry. Complete-active-space self-consistent field (CASSCF) calculations on each individual $Dy^{III}$ fragment (see Fig. S10 for the calculated model structures of **4_*a*** and **4_*b***) on the basis of single-crystal X-ray determined geometry have been carried out with MOLCAS 8.2 program package. Each individual $Dy^{III}$ fragment in **4_*a*** and **4_*b*** was calculated keeping the experimentally determined structure of the corresponding compound while replacing the neighboring $Dy^{3+}$ ion by diamagnetic $Lu^{3+}$.

The basis sets for all atoms are atomic natural orbitals from the MOLCAS ANO-RCC library: ANO-RCC-VTZP for $Dy^{III}$; VTZ for close N and O; VDZ for distant atoms. The calculations employed the second order Douglas-Kroll-Hess Hamiltonian, where scalar relativistic contractions were taken into account in the basis set and the spin-orbit couplings were handled separately in the restricted active space state interaction (RASSI-SO) procedure. Active electrons in 7 active spaces include all *f* electrons (CAS(9 in 7 for $Dy^{III}$)) in the CASSCF calculation. To exclude all the doubts, we calculated all the roots in the active space. We have mixed the maximum number of spin-free state which was possible with our hardware (all from 21 sextets, 128 from 224 quadruplets, 130 from 490 doublets). SINGLE_ANISO program was used to obtain the energy levels, ***g*** tensors, $m_J$ values, magnetic axes, *et al.,* based on the above CASSCF/RASSI-SO calculations.

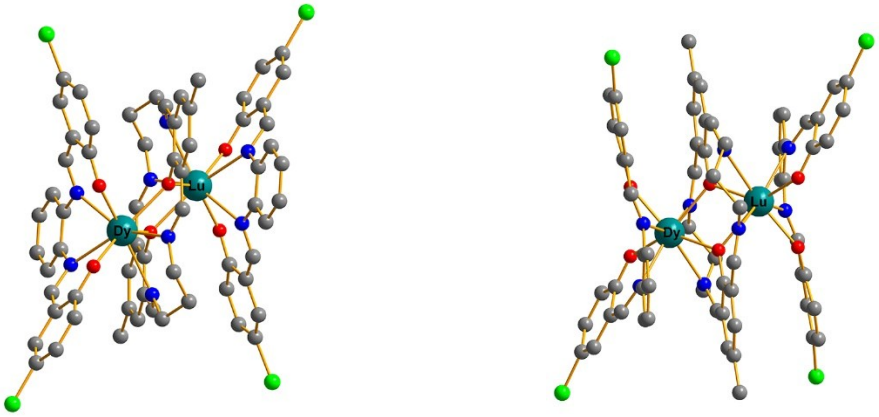


**4_*a*** **4_*b***

**Fig. S10** Calculated model structures of **4_*a*** and **4_*b*** for Dy complex **4** with hydrogen atoms and solvent molecule omitted for clarity.

**Table S5** Calculated energy levels ($cm^{-1}$), ***g*** ($g_x$, $g_y$, $g_z$) tensors and predominant $m_J$ values of the lowest eight Kramers Doublets (KDs) of **4_*a*** and **4_*b*** using CASSCF/RASSI-SO with MOLCAS 8.2.

| KDs | **4_*a*** | | | **4_*b*** | | |
|---|---|---|---|---|---|---|
| | $E/cm^{-1}$ | ***g*** | $m_J$ | $E/cm^{-1}$ | ***g*** | $m_J$ |
| 1 | 0.0 | 0.150<br>0.541<br>17.516 | ±15/2 | 0.0 | 0.076<br>0.262<br>17.271 | ±15/2 |
| 2 | 52.7 | 0.154<br>0.629<br>14.993 | ±13/2 | 49.0 | 0.097<br>0.341<br>14.756 | ±13/2 |
| 3 | 168.7 | 3.171<br>5.034<br>11.762 | ±11/2 | 162.6 | 1.581<br>2.619<br>12.630 | ±11/2 |
| 4 | 225.3 | 2.373<br>4.815<br>9.198 | ±7/2 | 214.2 | 3.520<br>5.940<br>8.768 | ±7/2 |
| 5 | 286.3 | 0.785<br>2.513<br>12.697 | ±5/2 | 270.9 | 1.704<br>3.855<br>12.176 | ±5/2 |
| 6 | 374.3 | 0.016<br>1.320<br>15.092 | ±3/2 | 340.4 | 0.313<br>1.427<br>16.348 | ±1/2 |
| 7 | 419.0 | 0.169<br>0.548<br>17.239 | ±1/2 | 381.1 | 0.243<br>1.577<br>15.988 | ±3/2 |
| 8 | 453.5 | 0.176<br>0.815<br>17.265 | ±9/2 | 403.8 | 0.364<br>2.156<br>16.063 | ±9/2 |

**Table S6** Wave functions with definite projection of the total moment | $m_J$ > for the lowest two KDs of individual $Dy^{III}$ fragments for **4_*a*** and **4_*b*** using CASSCF/RASSI-SO with MOLCAS 8.2.

| | $E/cm^{-1}$ | wave functions |
|---|---|---|
| **4_*a*** | 0.0 | 22.46%\|±15/2>+40.34%\|±13/2>+12.96%\|±11/2>+17.51%\|±9/2> |
| | 52.7 | 5.61%\|±13/2>+46.59%\|±11/2>+6.43%\|±9/2>+28.55%\|±7/2>+6.81%\|±5/2> |
| **4_*b*** | 0.0 | 33.37%\|±15/2>+24.59%\|±13/2>+22.68%\|±11/2>+13.66%\|±9/2> |
| | 49.0 | 45.98%\|±13/2>+9.59%\|±11/2>+34.95%\|±9/2>+5.38%\|±7/2> |

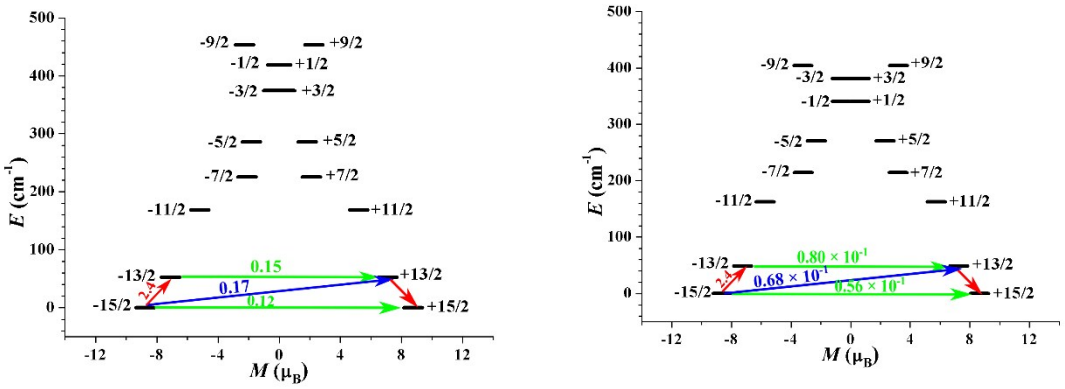


**4_*a*** **4_*b***

**Fig. S11** Magnetization blocking barriers for individual $Dy^{III}$ fragments in **4_*a*** and **4_*b***. The thick black lines represent the KDs of the individual $Dy^{III}$ fragments as a function of their magnetic moment along the magnetic axis. The green lines correspond to diagonal quantum tunneling of magnetization (QTM); the blue line represent Orbach relaxation processes. The path shown by the red arrows represents the most possibly path for magnetic relaxation in the corresponding compounds. The numbers at each arrow stand for the mean absolute value of the corresponding matrix element of transversal magnetic moments.

To fit the exchange interactions in **4_*a*** and **4_*b***, we took two steps to obtain them. Firstly, we calculated individual $Dy^{III}$ fragments using CASSCF/RASSI-SO to obtain the corresponding magnetic properties. Then, the exchange interaction between the magnetic centers is considered within the Lines model, while the account of the dipole-dipole magnetic coupling is treated exactly. The Lines model is effective and has been successfully used widely in the research field of *d* and *f*-elements single-molecule magnets.

For each of complexes **4_*a*** and **4_*b***, there is only one type of *J*.

The Ising exchange Hamiltonian is:

$$\hat{H}_{exch} = -J_{total}\hat{S}_{Dy1}\cdot\hat{S}_{Dy2}$$

The $J_{total}$ is the parameter of the total magnetic interaction ($J_{total} = J_{diploar} + J_{exchange}$) between magnetic center ions. The $\hat{S}_{Dy}$ = 1/2 is the ground pseudospin on the $Dy^{III}$ sites. The dipolar magnetic coupling can be calculated exactly, while the exchange coupling constants were fitted through comparison of the computed and measured magnetic susceptibility using the POLY_ANISO program.

**Table S7** Exchange energies $E$ ($cm^{-1}$), the energy difference between each exchange doublets $\Delta_t$ ($cm^{-1}$) and the main values of the $g_z$ for the lowest two exchange doublets of **4_*a*** and **4_*b***.

| | **4_*a*** | | | **4_*b*** | | |
|---|---|---|---|---|---|---|
| | $E$ | $\Delta_t$ | $g_z$ | $E$ | $\Delta_t$ | $g_z$ |
| 1 | 0.00 | $1.2\times10^{-3}$ | 35.072 | 0.00 | $1.6\times10^{-4}$ | 34.577 |
| 2 | 1.75 | $1.5\times10^{-3}$ | 0.000 | 1.96 | $2.0\times10^{-4}$ | 0.000 |

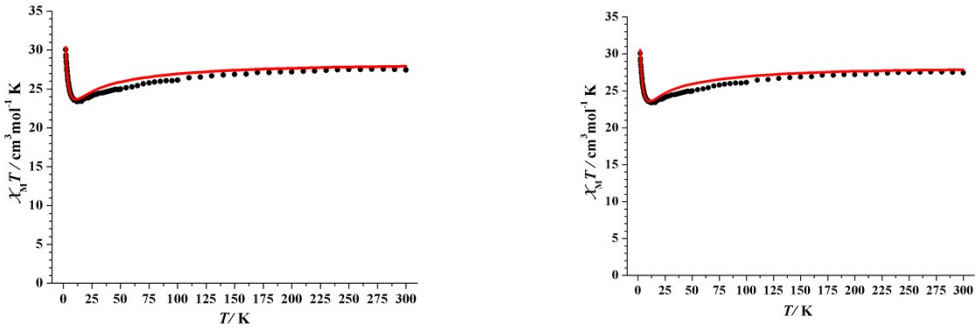


**4_*a*** **4_*b***

**Fig. S12** Calculated (red solid line) and experimental (black circle dot) data of magnetic susceptibilities of **4_*a*** and **4_*b***. The intermolecular interactions $zJ'$ of **4_*a*** and **4_*b*** were both fitted to 0.00 $cm^{-1}$.